Masataka Kinjo					
Maya Hirose, Hideki Tohda, Yuko Giga-Hama, Reiko Tsushima, Tamotsu Zako, Ryo Iizuka, Changi Pack, Masataka Kinjo, Noriyuki Ishii, and Masafumi Yohda	Interaction of a small heat shock protein of the fission yeast, Schizosaccharomyces pombe, with a denatured protein at elevated temperature	J. Biol. Chem	280	32586-32593	2005
Takashi Jin, Fumihiko Fujii, Hiroshi Sakata, Mamoru Tamura and Masataka Kinjo	Amphiphilic p-sulfonatocalix[4]arene-coated CdSe–ZnS quantum dots for the optical detection of the neurotransmitter acetylcholine	Chem. Commun		4300-4302	2005
Yasuo Takahashi, Ryuji Sawada, Kiyochika Ishibashi, Sintarou Mikuni and Masataka Kinjo	Analysis of Cellular Functions by Multipoint Fluorescence Correlation Spectroscopy	Current Pharmaceutical Biotechnology	6	159-156	2005
Takashi Jin, Fumihiko Fujii, Hiroshi Sakata, Mamoru Tamura and Masataka Kinjo	Calixarene-coated water-soluble CdSe/ZnS semiconsuctor quantum dots that are highly fluorescent and stable in aqueous solution,	Chem. Commun		2829-2831	2005
星美奈子	分子の探索からシステムの解明へーアルツハイマー病研究に想う神経科学の今後への私感	繊維と工業	62	17-18	2006
奈良優子, 村松慎一	パーキンソン病の再生医療．特集 治療の最前線：神経疾患の先端的治療	BRAIN MEDICAL	17(3)	41-45	2005
中林孝和、飯森俊文、金城政孝、太田信廣	蛍光寿命イメージングシステムの作成と生体試料および高分子試料への応用	分光研究	**55**	31-39	2006

IV. 研究成果の刊行物・別刷り

低温生物工学会誌〔Cryobiology and Cryotechnology〕, Vol. 51 , 137-140 , ,2005

β-アミロイド凝集に及ぼすトレハロースの効果

[1]東京工業大学バイオ研究基盤支援総合センター, [2]東京工業大学フロンティア創造共同研究センター
[3]東京工業大学大学院生命理工学研究科, [4]三菱化学生命科学研究所アルツハイマー病研究グループ
渡邉　亜沙子[1], 岡畑　恵雄[2,3], 古澤　宏幸[3], 星　美奈子[3,4], 櫻井　実[1]

The Effect of Trehalose on the Aggregation of β-amyloid

Asako WATANABE , Yoshio OKAHATA[2,3], Hiroyuki FURUSAWA[3], Minako HOSHI[3,4] and Minoru SAKURAI[1]

[1]Center for Biological Resources and Informatics, Tokyo Institute of Technology, 4259 Nagatsuta-cho, Midori-ku, Yokohama 226-8501, Japan

[2]Frontier Collaborative Research Center, Tokyo Institute of Technology, 4259 Nagatsuta-cho, Midori-ku, Yokohama 226-8501, Japan

[3]Department of Biomolecular Engineering, Tokyo Institute of Technology, 4259 Nagatsuta-cho, Midori-ku, Yokohama 226-8501, Japan

[4]Research Group for Alzheimer's Disease, Mitsubishi Kagaku Institute of Life Sciences, 11 Minamiooya, Machida, Tokyo 194-8511, Japan

The effect of trehalose on the aggregation of β-amyloid (Aβ) was investigated using quartz crystal microbalance (QCM) and circular dichroism spectroscopy (CD). Here we prepared three types of host Aβ-guest Aβ systems differing in a combination of their secondary structures: namely, β-sheet-β-sheet (system ①), β-sheet-random coil (system②) and random coil-random coil (system③). The host Aβ was fixed on the electrode of QCM, and the guest Aβ was dissolved in a buffer solution. The host-guest interaction was monitored through a frequency shift (ΔF) of the quartz vibration: a larger ΔF value means the occurrence of a larger degree of host-guest aggregation. When disaccharide (trehalose, neotrehalose or maltose) was added in the above system, the time dependent profile of ΔF was significantly affected. In systems ① and ②, any of these disaccharides depressed significantly the host-guest aggregation: maltose and trehalose exhibited the strongest effect in systems ① and ②, respectively. Interestingly, in system③, trehalose rather promoted the aggregation compared with the control (without disaccharide), while both maltose and neotrehalose depressed the aggregation as much as in the cases of systems ① and ②. The results of systems ② and ③ imply that trehalose more strongly interacts with Aβ in a random coil than that in β-sheets. In fact, CD measurements indicated that trehalose retarded the transformation of Aβ from a random coil to β-sheet. Taken together, these results open up the possibility that trehalose modifies the aggregation process of Aβ through its preferential interaction with the random coil state of A β.

(Received Oct. 27, 2005; Accepted 2005)

第51回低温生物工学研究報告15
[Key words : Trehalose, β-amyloid, aggregation, Quartz Crystal Microbalance, Circular Dichroism spectroscopy]

緒　言

トレハロースは乾燥・凍結などの水ストレスに対して保護作用を示すだけでなく，不飽和脂肪酸に対する酸化抑制作用[1]，さらに最近ではハンチントン病原因蛋白質に対する凝集抑制作用[2]も見出されており，この糖の多彩な交差耐性効果が注目を集めている．おそらくトレハロースはタンパク質や細胞膜表面との直接的な相互作用を通してこれらの機能を発現すると思われるが，そのメカニズムについては不明な点が多い．本研究では，アルツハイマー病の異常蓄積タンパク質として知られている β-アミロイド(Aβ) をモデルに，トレハロースが凝集過程に及ぼす影響を調べることで，この糖が蛋白質構造に与える影響，蛋白質安定化作用について基礎的知見を得ることを目的とした．Aβ の凝集過程は複雑であり，Aβ 分子種，濃度，溶媒条件等の違いにより，オリゴマー，線維，ADDLs，プロトフィブリル，アミロスフェロイド等の様々な凝集体を形成する．そこで本研究では，特に初期凝集過程に対するトレハロースの影響を，水晶発振子マイクロバランス法(QCM)と円偏光二色性(CD)を用いて解析した．

材料および方法

QCM は，金基板上に固定したホスト分子に対する，測定系内に加えたゲスト分子の結合を発振子の振動数変化として検出するもので，結合過程を経時的に観測できる．(Fig.1)

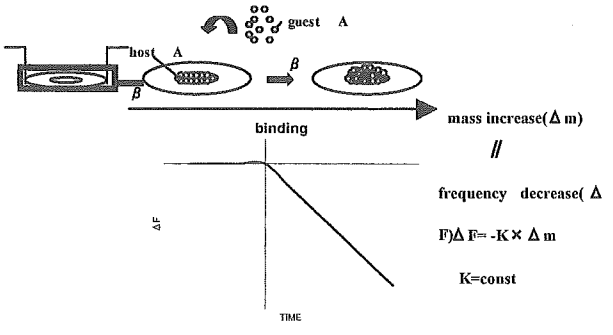

Fig. 1. Schematic diagram of QCM

本研究では，次の 3 つの系に対するトレハロース添加の効果を調べた．すなわち，①β シート構造の Aβ 同士の凝集，②基板上に固定した β シート構造の Aβ とランダムコイル構造の Aβ の凝集，③ランダムコイル構造の Aβ 同士の凝集である．比較対照として，ネオトレハロース，マルトースの添加実験も行った．まず，Aβ を QCM セルの基板に固定する．固定化法は系により 2 種類用いた．一つ目は，カチオン性の基板上に Aβ 溶液を滴下することで，中性付近で負に帯電している Aβ を静電的に固定する方法である．ここで，カチオン性基板は S 原子をもつ 2-アミノエタンチオール塩酸塩水溶液中に所定時間基板を浸漬させることにより作成した．もう一つの方法では、Aβ 溶液を所定時間基板と接触させることで，Aβ に含まれる S 原子と金基板を相互作用させて物理的に固定を行った．以上のいずれかの方法で Aβ を基板に固定した後，セルに溶媒 500μl を充填した．装置が安定化するのを待ち，二糖の溶液をセル内の濃度が 1mM となるよう測定系内に加え，装置付属の攪拌子で 5 秒間だけ攪拌した．さらに装置が安定化するのを待ち，Aβ 溶液を測定系内に加えて，測定を行った．この時の攪拌方法は Aβ 溶液を加えたときに数回ピペッティングする方法をとった．QCM 装置は株式会社イニシアム製 AFFINIX Q4 を用いた．Aβ は 40 残基の Aβ1-40, 42 残基の Aβ1-42 を用い，株式会社ペプチド研究所から購入した．これらは 70%アセトニトリル（株式会社メルク），0.05%トリフルオロ酢酸（株式会社ペプチド研究所）で凍結乾燥したのち使用直前に溶媒で 1mM になるよう溶解し，同じ溶媒で使用する濃度に希釈して用いた．溶媒として選択したリン酸緩衝生理食塩水(PBS)は日水製薬株式会社から，酢酸緩衝液の作製に使用した酢酸は和光純薬，酢酸ナトリウムは関東化学株式会社から購入した．トレハロース，ネオトレハロースは株式会社林原生物化学研究所から提供していただいた．マルトースは関東化学株式会社から購入した．①～③の各系に対する実験条件は Table 1 に示した．

次に，CD スペクトルを用いて溶液中の Aβ の二次構造を調べた．測定に使用した溶液は Aβ1-40 の 30μM 溶液で，溶媒はリン酸緩衝生理食塩水 (pH 7.4) (PBS)である．トレハロースを加える場合，濃度

は 1mM とした．CD 装置は（株）日本分光製 J-720 spectropolarimeter，セルは光路長 0.1cm の石英製セル（GL サイエンス製）を用いた．

Table1. Experimental conditions of QCM measurements

		system①	system②	system③
Buffer		acetate buffer (pH 5.0)	acetate buffer (pH 5.0)	PBS (pH 7.4)
host Aβ		$Aβ_{1-42}$	$Aβ_{1-42}$	$Aβ_{1-40}$
	Secondary structure	β-sheet	β-sheet	random coil
	immobilization method	Physical	physical	electrostatic
	concentration	25μM	25μM	4μM
guest Aβ		$Aβ_{1-42}$	$Aβ_{1-40}$	$Aβ_{1-40}$
	Secondary structure	β-sheet	random coil	random coil
	concentration	10μM	1μM	1μM

結果と考察

Fig.1 で示した通り QCM の振動数変化と基板上の質量変化は比例関係にあり，振動数減少幅が大きいほど基板上の質量増大が大きいといえる．したがって，本研究のホストーゲスト系 system①～③において，基板上のホストへのゲスト分子の凝集が起こるならば，その進行にともない QCM の振動数減少が観測されるだろう．また，糖添加の効果は，一定時間経過後の振動数減少幅あるいは減少速度を比較することにより評価することができると考えられる．

Fig.2.a-c はそれぞれ system①～③に対する QCM 実験の結果を示す．各図において trehalose，neotrehalose, maltose はこれら二糖を添加した測定系の結果を示し，control は糖無添加系に対する結果を示す．

system①の糖無添加系では，約 150 分経過後 750Hz 程度の振動数減少が観測された．一方，トレハロース，ネオトレハロース，マルトースを添加系では，ほぼ同一時間経過後，それぞれ 670，750，540Hz 程度の振動数減少が観測された．したがって，ホスト，ゲストいずれも β シート構造 Aβ をもつ system①では，マルトースが最も高い凝集抑制効果を示すことが判明した．

それに対し system②では，150 分経過後の振動数減少幅は，糖無添加，トレハロース，ネオトレハロース，マルトースについて，それぞれ 390，200，410，310Hz であり，β シート構造の Aβ とランダムコイルの Aβ の凝集に関しては，トレハロースが最も高い凝集抑制効果をもつことが確認された．

興味あることに，ランダムコイル構造の Aβ 同士の凝集に対応する system③では，トレハロースを添加すると，糖無添加系に比べて振動数減少値が大きくなることが観測された．一方，ネオトレハロースとマルトースを添加した測定系では，system①と②の場合と同じく，糖無添加系に比べて振動数減少幅の減少が見られた．これらの結果は，ランダムコイル構造の Aβ 同士の凝集に関して，マルトースとネオトレハロースは凝集抑制効果をもつが，トレハロースはより重量の大きな凝集体形成を促進する効果をもつことを示している．しかし，この system③については実験ごとに値が変動するため，添加した Aβ の金基板への非特異的吸着などを再検討する必要もあることを付記しておく．

以上より，トレハロースの Aβ 凝集に対する効果として次の 2 つの特徴が見出された．すなわち，1）トレハロースが高い凝集抑制効果を示すのは，ホスト，ゲストのうち一方がランダムコイルのときであ

る（system①と②の比較），2）ランダムコイル構造の Aβ 同士の凝集に対してトレハロースは他の二糖には無い特異的な効果をもつ（system③）．これらをまとめると，トレハロースはランダムコイル構造の Aβ に作用し，その凝集過程に有意な影響を与えると推定される．

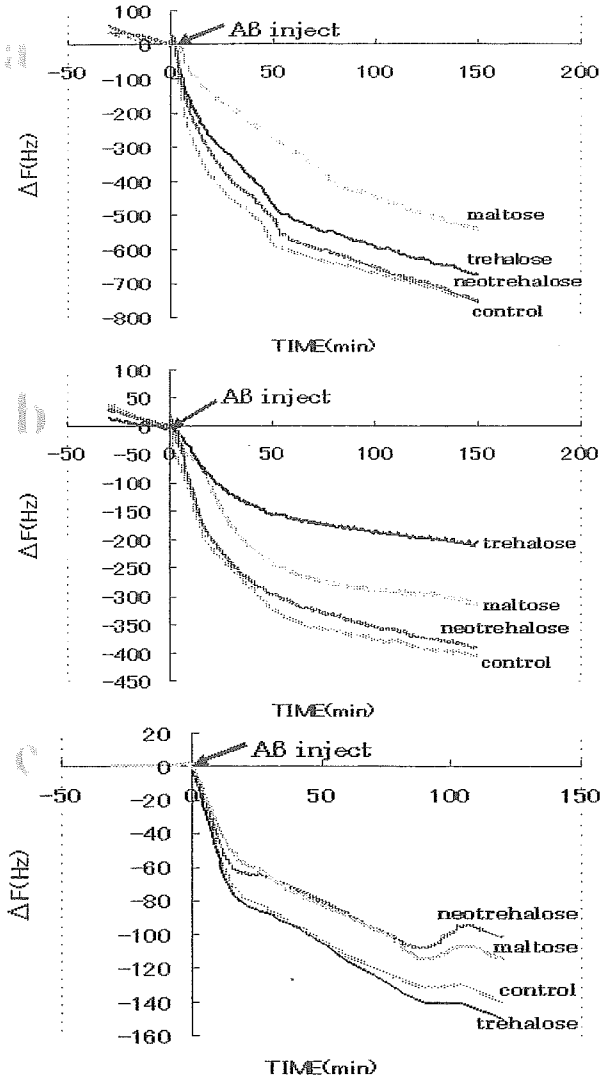

Fig. 2. Frequency shifts as a function of time during Aβ aggregation

そこで，トレハロースを添加した系と添加していない系それぞれに対して，Aβ がランダムコイル構造から β シート構造に変異するまでに要する時間を CD 測定より評価し比較した．トレハロースを添加していない系では，今回の測定条件においてランダムコイル構造から β シート構造への変異に要する時間が 190 時間だったのに対し，トレハロースを添加した系では 210 時間に延長されるこが確認できた．つまり，トレハロースは Aβ がランダムコイル構造から β シート構造への変異するのを抑制することが判明した．

ランダムコイル状態の Aβ では，親水基はもとより疎水基も水に露出していると考えられる．一方，最近のわれわれの研究によると，トレハロースは親水基のみならず，不飽和結合をもつ疎水基に特異的結合することが判明している[1,3]．これは他の二糖にはないトレハロース特有の性質である．したがって，system②や③の系では，トレハロースはおそらくランダムコイル Aβ の極性基のみならず疎水基とも水素結合を形成して安定化し，β シート構造への変異を抑制するとともに，凝集体の構造を変調しているのではないかと推測される．

謝辞

CD スペクトルの測定法をご指導してくださった東京工業大学大学院生命理工学研究科川崎剛美助手に深く感謝いたします．この研究は以下の研究費援助により行われた．本研究の一部は，生研センター基礎研究推進事業試験研究費（PROBRAIN）及び文部科学省科学研究費特定領域研究（no.16041212）により実施された．

文献

1) Oku, K., Watanabe, H., Kubota, M., Fukuda, S., Kurimoto,M., Tsujisaka, Y., Komori, M., Inoue, Y. and Sakurai, M. : NMR and Quantum Chemical Study on the OH…π and CH…O Interactions between Trehalose and Unsaturated Fatty Acids: *J. Am. Chem. Soc.*, **125**, 12739-12748 (2003)

2) Tanaka, M., Machida, Y., Niu, S., Ikeda, T., Jana, R N.,Doi, H., Kurosawa, M., Nekooki, M. and Nukina, N.: Trehalose alleviates polyglutamine-mediated pathology in a mouse model of Huntington disease: *Nature Med.*, **10**, 148-154 (2004)

3) Oku, M. Kurose, M., Kubota, S., Fukuda, M., Kurimoto, Y., Tujisaka, A., Okabe and Sakurai, M.: Combined NMR and Quantum Chemical Study on the Interaction between Trehalose and Diene

Relevant to the Antioxidant Function of Trehalose, *J. Phys. Chem. B*, **109**, 3032-3040 (2005)

Available online at www.sciencedirect.com
SCIENCE DIRECT®
Biochemical Pharmacology 69 (2005) 669–678
Biochemical Pharmacology
www.elsevier.com/locate/biochempharm

Assignment of voltage-gated potassium channel blocking activity to κ-KTx1.3, a non-toxic homologue of κ-hefutoxin-1, from *Heterometrus spinifer* venom

Selvanayagam Nirthanan[a,1], Joost Pil[b,1], Yousra Abdel-Mottaleb[b], Yuko Sugahara[c], Ponnampalam Gopalakrishnakone[d,*], Jeremiah S. Joseph[e], Kazuki Sato[c], Jan Tytgat[b]

[a]*Department of Neurobiology, Harvard Medical School, Boston, MA 02115, USA*
[b]*Laboratory of Toxicology, University of Leuven, 3000 Leuven, Belgium*
[c]*Fukuoka Women's University, Kasumigaoka, Higashi-ku, Fukuoka 813-8529, Japan*
[d]*Venom and Toxin Research Programme, Faculty of Medicine, National University of Singapore, Singapore 117597, Singapore*
[e]*The Scripps Research Institute, La Jolla, CA 92037, USA*

Received 19 July 2004; accepted 20 October 2004

Abstract

A new family of weak K^+ channel toxins (designated κ-KTx) with a novel "bi-helical" scaffold has recently been characterized from *Heterometrus fulvipes* (Scorpionidae) venom. Based on the presence of the minimum functional dyad (Y5 and K19), κ-hefutoxin-1 (κ-KTx1.1) was investigated and found to block Kv 1.2 (IC_{50} ~40 μM) and Kv 1.3 (IC_{50} ~150 μM) channels. In the present study, κ-KTx1.3, that shares ~60% identity with κ-hefutoxin 1, has been isolated from *Heterometrus spinifer* venom. Interestingly, despite the presence of the functional dyad (Y5 and K19), κ-KTx1.3 failed to reproduce the K^+ channel blocking activity of κ-hefutoxin-1. Since the dyad lysine in κ-KTx1.3 was flanked by another lysine (K20), it was hypothesized that this additional positive charge could hinder the critical electrostatic interactions known to occur between the dyad lysine and the Kv 1 channel selectivity filter. Hence, mutants of κ-KTx1.3, substituting K20 with a neutral (K20A) or a negatively (K20E) or another positively (K20R) charged amino acid were synthesized. κ-KTx1.3 K20E, in congruence with κ-hefutoxin 1 with respect to subtype selectivity and affinity, produced blockade of Kv 1.2 ($IC_{50} = 36.8 \pm 4.9$ μM) and Kv 1.3 ($IC_{50} = 53.7 \pm 6.7$ μM) but not Kv 1.1 channels. κ-KTx1.3 K20A produced blockade of both Kv 1.2 ($IC_{50} = 36.9 \pm 4.9$ μM) and Kv 1.3 ($IC_{50} = 115.7 \pm 7.3$ μM) and in addition, acquired affinity for Kv 1.1 channels ($IC_{50} = 110.7 \pm 7.7$ μM). κ-KTx1.3 K20R failed to produce any blockade on the channel subtypes tested. These data suggest that the presence of an additional charged residue in a position adjacent to the dyad lysine impedes the functional block of Kv 1 channels produced by κ-KTx1.3.

Keywords: Scorpion toxin; Voltage-gated potassium channel; Functional dyad; κ-Hefutoxin 1; κ-KTx1.3; *Heterometrus spinifer*

The venoms of the black scorpion *Heterometrus* spp. (Scorpionidae) including the Malaysian black scorpion (*Heterometrus spinifer*) have been reported to be of a lower order of toxicity in comparison to those from the Buthidae scorpions [1] from which highly potent neurotoxins that target Na^+ as well as various subtypes of K^+ channels have been isolated [2]. In contrast, mostly neurotoxins which modify K^+ channel activity, the role of which is presumed to be of minor consequence in lethal envenomation, have been found to be present in low quantities in the venoms of some Scorpionidae members [3–5]. Scorpion toxins that target K^+ channels are compact peptides that typically contain 23–43 amino acid residues and three or four disulfide bridges [2,6,7]. Moreover, almost all of these toxins adopt a highly conserved

Abbreviation: K^+, potassium

* Corresponding author. Tel.: +65 687 43207; fax: +65 677 87643.
E-mail address: antgopal@nus.edu.sg (P. Gopalakrishnakone).

[1] Contributed equally to this work.

0006-2952/$ – see front matter © 2004 Elsevier Inc. All rights reserved.
doi:10.1016/j.bcp.2004.10.018

secondary structure, the cysteine-stabilized α/β-fold, which consists of a segment of an α-helix and a double- or triple-stranded β-sheet that are held together in a stable conformation by two or more disulfide bridges [2,7–10]. These toxins have been classified into three-subfamilies, called α-, β- and γ-KTxs [10–12].

We have recently reported the isolation and characterization of a 22-residue long peptide with weak K^+ channel blocking activity (IC_{50} ~40 to 150 μM), κ-hefutoxin 1, from *Heterometrus fulvipes* venom that adopts a novel fold comprising of two parallel α-helices cross-linked by two disulfide bridges [13]. Interestingly, the K^+ channel blocking activity of κ-hefutoxin 1 was deduced following its structural characterization that revealed the presence of two key residues, tyrosine and lysine at positions 5 and 19, respectively, positioned at a distance of~6.0 Å between the lysine's α-carbon and the center of the aromatic face of the tyrosine [13]. Such a critically positioned dyad, composed of a positively charged amino acid and a hydrophobic residue, is well-known to constitute the minimum functional requirement for K^+ channel blocking activity of a variety of toxins isolated from venoms across different phyla [13–15].

We have now isolated a new 23-residue peptide from the venom of *H. spinifer* that shares ~60% identity with κ-hefutoxin 1, and based on sequence similarity, was identified as the third member of the κ-KTx subfamily and hence designated as κ-KTx1.3. However, despite the presence of the putative functional dyad (Y5 and K19) in identical positions in its sequence, κ-KTx1.3 failed to reproduce the blocking activity of κ-hefutoxin 1 on Kv 1.2 and Kv 1.3 channels. On analyzing the primary structure of κ-KTx1.3, it was found that the critical lysine (K19) was flanked by another lysine (K20) and it was postulated that this additional positive charge may hinder critical electrostatic interactions reported to occur between the dyad lysine extremity and the carbonyl oxygen atoms of conserved residues in the Kv 1 channel selectivity filter. We have therefore, chemically synthesized mutants of κ-KTx1.3 substituting the flanking lysine with a neutral amino acid (K20A) or a negatively charged glutamic acid (K20E) as found in κ-hefutoxin 1. Interestingly, by these single-residue substitutions, we were able to assign K^+ channel blocking activity to a scorpion venom-derived peptide that was otherwise inactive on Kv channels.

1. Materials and methods

1.1. Materials

H. spinifer venom was extracted from live scorpions maintained in captivity in the Venom and Toxin Research Laboratory, National University of Singapore as described previously [16]. Pre-packed chromatography columns were purchased from Pharmacia Biotech. All drugs and chemicals were purchased from Sigma Chemicals with the exception of the following, which were obtained from the sources indicated: reagents for N-terminal sequencing, acetonitrile (Fisher Scientific) and trifluoroacetic acid (Fluka Chemika-Biochemika). HPLC-grade water was obtained by using a Milli-Q purification system (Millipore).

1.2. Purification of κ-KTx1.3

Pooled scorpion venom was subjected to ultra-filtration using Mr = 5000 micro-concentrators (Amicon). The venom (500 μl) was transferred to the sample reservoir of the microconcentrator and centrifuged at 4500 × *g* for 90 min at 4 °C. The filtrate of Mr < 5000 was then subjected to a single-step reverse phase HPLC using a Sephasil C8 (0.21 cm × 10 cm) column using a Vision Biocad Workstation (Bio-Rad Laboratories). The column was equilibrated with 0.1% trifluoroacetic acid and the proteins were eluted with a linear gradient (20–50% over 80 min) of eluant (80% acetonitrile in 0.1% trifluoroacetic acid). Elution of proteins was monitored at 215 nm.

1.3. Mass spectrometry

Purified κ-KTx1.3 was subjected to electrospray ionization mass spectrometry as described previously [16] using a Perkin-Elmer Sciex API 300 triple quadrupole instrument (Sciex) equipped with an ion-spray interface. The ion-spray and orifice voltages were set to 4600 and 30 V, respectively. Nitrogen was used as curtain gas with a flow rate of 0.6 l/min while compressed air was used as a nebulizer gas. The sample was infused by flow injection at a flow rate of 50 μl/min using Shimadzu 10 AD pumps as the solvent delivery system. Matrix-assisted laser desorption ionisation–time of flight (MALDI–TOF) mass spectrometry was performed on a Voyager DE-STR Biospectrometry Workstation (Applied Biosystems). Saturated sinapinic acid (3,5-dimethoxy-4-hydroxycinnamic acid) (10 mg/ml) in 1:1 acetonitrile:water containing 0.3% trifluoroacetic acid was used as the matrix. The sample (~5 pmol in 1 μl) was spotted onto a stainless steel sample plate with 1 μl of matrix solution and dried off. Molecular ions were generated using a nitrogen laser (337 nm) at an intensity of 1800–2200 and extraction of ions was delayed by 800 ns. The accelerating voltage was set at 25,000 V and the grid and guide wire voltages at 93.0 and 0.3%, respectively. The spectrum was calibrated using external standards.

1.4. Determination of the N-terminal amino acid sequence

Amino terminal sequencing of the native and pyridylethylated protein was done by automated Edman degrada-

tion using a Perkin-Elmer Applied Biosystems 494 pulsed-liquid phase protein sequencer (Procise) with an on-line 785A phenylthiohydantoin-derivative analyzer. For pyridylethylation, native κ-KTx1.3 was re-suspended in 100 μl of denaturant buffer (6.0 M guanidinium hydrochloride, 0.13 M Tris, 1 mM EDTA, pH 8.0) containing 0.07 M β-mercaptoethanol and heated at 37 °C for 2 h. Subsequently, 1.5-fold molar excess (over sulfhydryl groups) of 4-vinylpyridine was added and incubated at room temperature for 2 h, after which the sample was desalted by reverse phase HPLC.

1.5. Peptide synthesis

Linear precursors of κ-KTx1.3 with free (κ-KTx1.3(OH)) and amidated (κ-KTx1.3(NH_2)) carboxy terminals as well their analogues (κ-KTx1.3 K20A, κ-KTx1.3 K20E and κ-KTx1.3 K20R) were synthesized by solid phase methodology with Fmoc chemistry on an Applied Biosystems (model 433A) peptide synthesizer, oxidized by air oxidation and purified by HPLC as described previously [13]. The structures and purity of the synthetic peptides and native κ-KTx1.3 were confirmed by HPLC co-injection analysis and MALDI–TOF mass spectrometry measurements. In order to determine the disulfide pairings, synthetic κ-KTx1.3(OH) (0.4 mg) was dissolved in 0.4 ml of 0.1 M phosphate buffer pH 6.5) and digested with trypsin (0.1 mg at 37 °C for 3 h). The digested peptide fragments were separated by HPLC and subjected to MALDI–TOF mass spectrometry measurements.

1.6. Molecular modeling

The NMR structure of κ-hefutoxin 1 (PDB accession number 1HP9; first out of the ensemble of 20 lowest energy structures) from *H. fulvipes* was used as the template for comparative molecular modeling of κ-KTX1.3. The molecular model was constructed using InsightII (Molecular Simulations Inc., USA) as described previously [17].

1.7. Expression in Xenopus oocytes

Kv 1.1 (rat), Kv 1.2 (rat) and Kv 1.3 (human) channels were studied. Plasmids containing Kv 1.1 were first linearized with PstI (New England Biolabs) 3′ to the 3′ non-translated β-globin sequence in a custom-made high expression vector for oocytes, pGEM-HE [18] and then transcribed using Ambion's mMESSAGE mMachine T7 transcription kit (Ambion). The cDNA encoding Kv 1.2 in its original vector, pAKS2, was first subcloned into pGEM-HE [18]. The insert was released by double restriction digest with *Bgl*II and *Eco*RI and ligated into the *Bam*HI and *Eco*RI sites of pGEM-HE. For in vitro transcription, the cDNA was linearized with *Sph*I and transcribed using the large-scale T7 mMESSAGE mMACHINE transcription kit (Ambion). The plasmids pCI.neo containing the gene for Kv 1.3 were linearized with *Not*I (Promega) and transcribed like Kv 1.2. Stage-V and -VI *Xenopus laevis* oocytes were harvested by partial ovariectomy under anaesthesia (3-aminobenzoic acid ethyl ester methanesulfonate salt, 0.5 g/l, Sigma). Anaesthetized animals were kept on ice during dissection. The oocytes were defolliculated by treatment with 2 mg/ml collagenase (Sigma) in Ca^{2+}-free ND-96 solution (in mM: NaCl 96, KCl 2, $MgCl_2$ 1, HEPES 5 adjusted to pH 7.5). Between 1 and 24 h after defolliculation, oocytes were injected with 10 nl of 50–100 ng/μl cRNA. The oocytes were then incubated in ND-96 solution (supplemented with 50 mg/ml gentamycin sulphate) at 16 °C for one day.

1.8. Electrophysiological measurements

Two-electrode voltage-clamp recordings were performed at room temperature using a GeneClamp 500 amplifier (Axon Instruments) controlled by a pClamp data acquisition system (Axon Instruments). Whole-cell currents from oocytes were recorded 1 day after injection. Voltage and current electrodes were filled with 3 M KCl. Resistances of both electrodes were kept as low as possible (<0.5 MΩ). Bath solution composition was (in mM): NaCl 96, KCl 2, $CaCl_2$ 1.8, $MgCl_2$ 2 and HEPES 5 (pH 7.4). Using a four-pole low-pass Bessel filter, currents were filtered at 1 kHz and sampled at 2 kHz. Current traces were evoked in an oocyte expressing Kv channels by depolarizations to 0 mV from a holding potential of −90 mV. Statistical analysis between groups of data was carried out using the Student's *t*-test and a probability of <0.05 was considered to be statistically significant.

2. Results

2.1. Isolation and purification of κ-KTx1.3

Ultracentrifugation of *H. spinifer* resulted in a filtrate of Mr < 5000, which would likely contain the neurotoxins directed against K^+ channels. The venom ultrafiltrate was then directly subjected to reverse-phase HPLC which resulted in the separation of over 30 small peptides (Fig. 1A). The most prominent peak (identified by arrow) was subjected to mass spectrometry and found to contain a near-homogenous (~97% purity) peptide with a molecular mass of 2620.58 ± 0.55 Da (electrospray ionization mass spectrometry) (Fig. 1B) and 2620.71 Da (MALDI–TOF mass spectrometry) (data not shown). This peptide was subsequently identified as κ-KTx1.3.

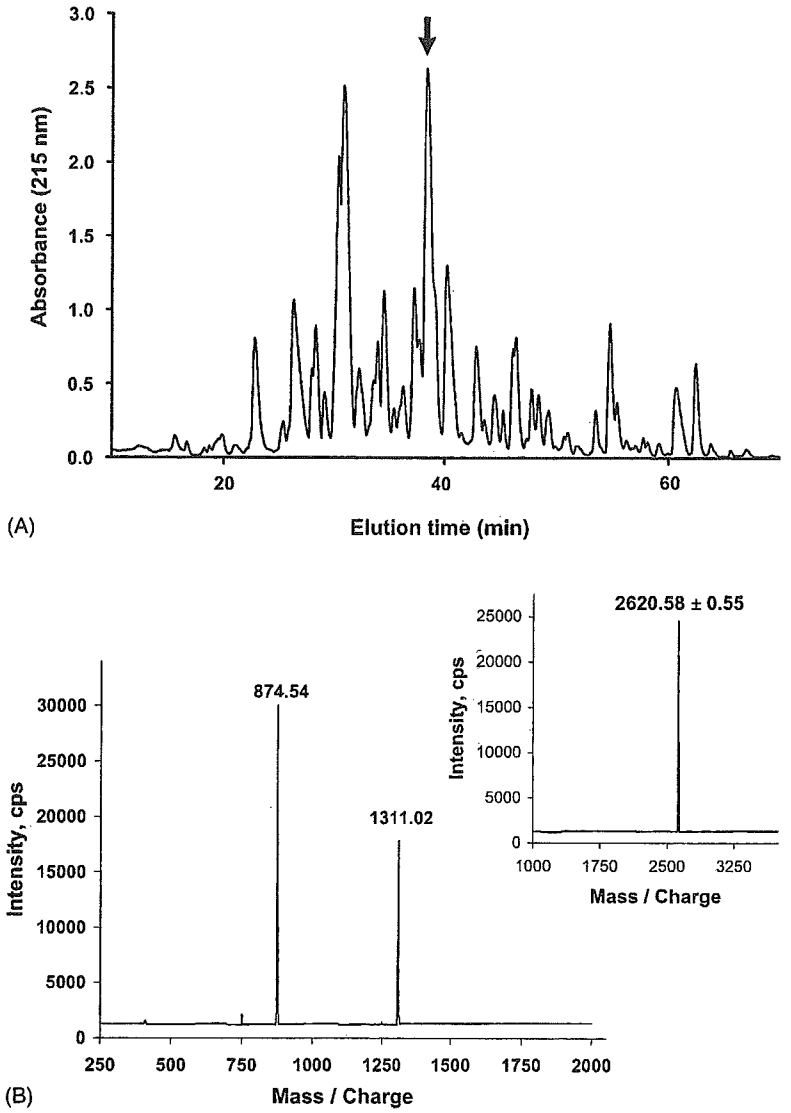

Fig. 1. Isolation and purification of κ-KTx1.3: (A) reverse-phase HPLC of *H. spinifer* venom ultrafiltrate (Mr < 5000) on a Sephasil C8 (0.21 cm × 10 cm) column equilibrated with 0.1% trifluoroacetic acid. Proteins were eluted with a linear gradient (20–50% over 80 min) of eluent (80% acetonitrile in 0.1% trifluoroacetic acid) at a flow rate of 1 ml/min. The elution of proteins was monitored at 215 nm. The peak indicated by arrow was identified as κ-KTx1.3 and subjected to mass spectroscopy, (B) electrospray ionization mass spectrum of κ-KTx1.3 shows a series of multiply charged ions, corresponding to a single, homogenous peptide of molecular mass 2620.58 ± 0.55 Da (inset, reconstructed spectrum).

2.2. Determination of the amino acid sequence of κ-KTx1.3

We were able to unequivocally identify all the residues and determine the complete amino acid sequence of both native (blank cycles where cysteine residues are found) and pyridylethylated κ-KTx1.3. κ-KTx1.3 has 23 amino acid residues including four cysteine residues. Its calculated mass, with the expected two disulfide bridges, was 2620.91, which coincides well with the estimated molecular mass. It shared ~60% identity to κ-hefutoxin 1 (κ-KTx1.1) and κ-hefutoxin 2 (κ-KTx1.2) [13] and almost no sequence similarity to any other known scorpion toxins. Hence, κ-KTx1.3 was identified as the third member of the recently identified κ-KTx subfamily of weak K^+ channel toxins and was designated as κ-KTx1.3 (Fig. 2). The amino acid sequence of κ-KTx1.3 is deposited in the SWISS-PROT protein database (accession number P83655).

2.3. Solid phase synthesis of κ-KTx1.3

Due to the low yield (~0.1%) of native κ-KTx1.3, it was chemically synthesized for further characterization. Since κ-hefutoxin 1 and κ-hefutoxin 2 had amidated and free-carboxy termini, respectively, linear precursors of κ-KTx1.3 with both, amidated and free carboxy-termini, were synthesized by Fmoc solid phase method. Random air oxidation of the linear precursors of κ-KTx1.3 afforded a major product which was purified until it migrated as a single peak on analytical HPLC. The purity of synthetic

κ-KTx 1.1	Hefutoxin-1	GHACYRNCWREGNDEETCKERC
κ-KTx 1.2	Hefutoxin-2	GHACYRNCWREGNDEETCKERCG
κ-KTx 1.3	Native	GFGCYRSCWKAGHDEETCKKECS
κ-KTx 1.3	K20E	GFGCYRSCWKAGHDEETCKEECS
κ-KTx 1.3	K20A	GFGCYRSCWKAGHDEETCKAECS
κ-KTx 1.3	K20R	GFGCYRSCWKAGHDEETCKRECS
κ-KTx 1.1	Hefutoxin-1 E20K R21E	GHACYRNCWREGNDEETCKKEC

4 8 18 22

Fig. 2. Amino acid sequences of the members of the κ-KTx subfamily. The cysteines are numbered and the disulfide linkages outlined. The residues contributing to the functional dyad are in bold. The residues by which κ-KTx1.3 differs from κ-hefutoxin 1 are shaded in grey and the mutated residues in κ-KTx1.3 and κ-hefutoxin 1 are underlined. The Swiss-Prot (Swiss Institute for Bioinformatics) accession numbers are P82852, P82851 and P83655, respectively, for κ-hefutoxin 1 and 2 (*Heterometrus fulvipes*) and κ-KTx1.3 (*Heterometrus spinifer*). The International Union of Pure and Applied Chemistry one-letter notation for amino acids is used (*J Biol Chem* 1968;243:3557–9).

peptides was confirmed by analytical HPLC and MALDI–TOF mass spectrometry. Synthetic κ-KTx1.3 with either amidated or free carboxy-termini were co-injected with native κ-KTx1.3 on to an analytical HPLC which resulted in κ-KTx1.3 (OH), but not κ-KTx1.3 (NH_2), eluting together with the native peptide as a single peak (Fig. 3). This confirmed that κ-KTx1.3 has a free carboxyl group at its carboxy-terminal end.

2.4. Assignment of disulfide pairings in κ-KTx1.3

To determine the disulfide bond pairings, synthetic κ-KTx1.3 was digested with trypsin which yielded three digest products of MW 1639.60, 1511.53 and 1039.08 that agreed with the calculated MW for the digested fragments SCWKAGHDEETCKK + H_2O, SCWKAGHDEETCK + H_2O and GFGCYRECS + H_2O, respectively (Fig. 4). These data confirmed that κ-KTx1.3, like κ-hefutoxin-1 and 2 [13], also has disulfide combinations of C1–C4 and C2–C3 (Fig. 5A and 5B). The circular dichroism spectra of synthetic κ-KTx1.3 (OH) revealed that it has a conformation typical of α-helical structure (data not shown).

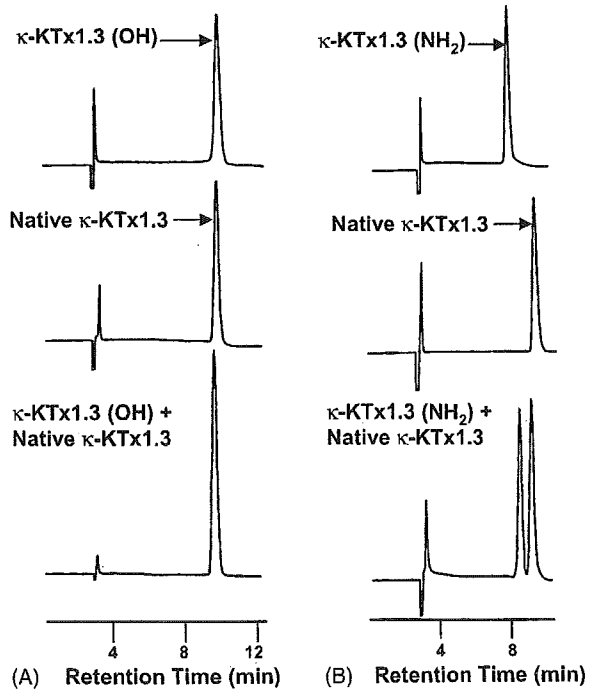

Fig. 3. Synthesis of κ-KTx1.3. Linear precursors of κ-KTx1.3 with free (κ-KTx1.3(OH)) and amidated (κ-KTx1.3(NH_2)) carboxy termini were synthesized by solid phase methodology with Fmoc chemistry. Synthetic κ-KTx1.3(OH) and κ-KTx1.3(NH_2) were co-injected with native κ-KTx1.3 on to an analytical HPLC which resulted in κ-KTx1.3 (OH) (A), but not κ-KTx1.3 (NH_2) (B), eluting together with the native peptide as a single peak. This confirmed that κ-KTx1.3 has a free carboxyl group at its carboxy-terminal end.

2.5. Molecular modeling of κ-KTx1.3

Since κ-KTx1.3 shared ~60% identity in primary sequence including disulfide pairing with κ-hefutoxin 1, the NMR structure of the latter (PDB accession number 1HP9) was used as a template to create a molecular model of κ-KTx1.3. Like κ-hefutoxin 1, the model of κ-KTx1.3 revealed a compact structure consisting of two parallel α-helices that are held together by the two disulfide bridges (C4–C22 and C8–C18) (Fig. 5A and 5B). The K^+ channel blocking activity of κ-hefutoxin was deduced based on the presence of the minimum functional dyad, K19 and Y5, positioned at a distance of ~6.01 Å between the α-carbon of the lysine and the center of the aromatic face of the tyrosine (Fig. 5C) [13]. The model of κ-KTx1.3 also

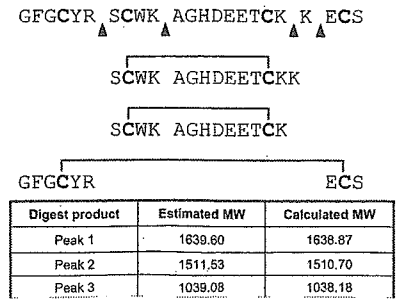

Digest product	Estimated MW	Calculated MW
Peak 1	1639.60	1638.87
Peak 2	1511.53	1510.70
Peak 3	1039.08	1038.18

Fig. 4. Assignment of disulfide pairings in κ-KTx1.3. To determine the disulfide bond pairings, synthetic κ-KTx1.3 was digested with trypsin which yielded three digest products of MW 1639.60, 1511.53 and 1039.08 that agreed with the calculated MW for the digested fragments SCWKAGHDEETCKK + H_2O, SCWKAGHDEETCK + H_2O and GFGCYRECS + H_2O, respectively. These data confirmed that κ-KTx1.3 has disulfide combinations of C1–C4 and C2–C3.

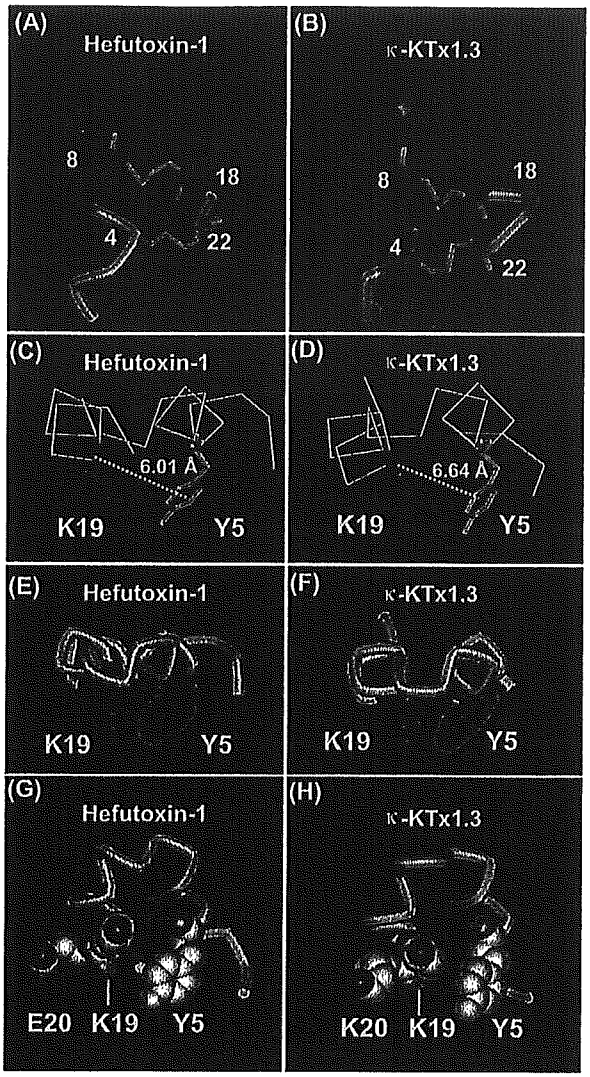

Fig. 5. Molecular model of κ-KTx 1.3. The NMR structure of κ-hefutoxin 1 (A) (PDB accession number 1HP9; first out of the ensemble of 20 lowest energy structures) was used as a template to construct a molecular model of κ-KTX1.3 (B) using InsightII (Molecular Simulations Inc., USA). Like κ-hefutoxin 1, the model of κ-KTx1.3 revealed a compact structure consisting of two parallel α-helices that are held together by the two disulfide bridges (C4–C22 and C8–C18) (shown in green). The K^+ blocking activity of κ-hefutoxin 1 was deduced based on the presence of the functional dyad, Y5 and K19, positioned at a distance of 6.01 Å between the α-carbon of the lysine and the center of the aromatic face of the tyrosine (C). The molecular model of κ-KTX1.3 also showed the presence of this dyad (Y5, K19) positioned at a distance of 6.64 Å (D). The α-carbon backbone structure is presented in C and D. In both, κ-hefutoxin 1 (E) and κ-KTX1.3 (F), the dyad residues (shown in Corey–Pauling–Koltun presentation) K19 (violet) and Y5 (green) protrude out of a flat surface formed by the edges of the two parallel α-helices, in conformity with the general architecture of other pore-blocking K^+ channel toxins. The amino acid residue at position 20, Glu20 in κ-hefutoxin 1 (G) and Lys20 in κ-KTX1.3 (H) is also shown in relation to the functional dyad (K19, Y5) in the respective toxins. In (G) and (H), both toxins are shown in similar orientations along the long-axis of the side chain of K19 with the selected residues in Corey–Pauling–Koltun representation. The amino acid residues are coloured according to their charge, with blue and red depicting positive and negative charge, respectively. (For interpretation of the references to colour in this figure legend, the reader is referred to the web version of the article.)

revealed the presence of this functional dyad (K19/Y5) which were positioned at a comparable distance of 6.64 Å between them (Fig. 5D). As observed in κ-hefutoxin 1 (Fig. 5E), both K19 and Y5 in κ-KTx1.3 also protrude out of a flat surface formed by the edges of the two parallel α-helices (Fig. 5F). These data strongly suggested that the molecular targets of κ-KTx1.3 could also be voltage-gated K^+ channels.

2.6. Biological activity of κ-KTx1.3

Synthetic κ-KTx1.3 was screened for K^+ channel blocking activity in *X. laevis* oocytes expressing a single type of voltage-gated K^+ channel (Kv 1.1, Kv 1.2 or Kv 1.3). κ-KTx1.3 did not inhibit currents through Kv 1.1, Kv 1.2 or Kv 1.3 channels even at high concentrations of 1 mM (see Fig. 6) suggesting that it was functionally inert on Kv 1 channels.

2.7. Rationale for the synthesis of mutants of κ-KTx1.3

On analyzing the primary sequences of κ-KTx1.3 and κ-hefutoxins 1 and 2, it was found that the functional dyad lysine (K19) in κ-KTx1.3 was flanked by another lysine (K20) (Figs. 2 and 5). Experimental and modeling data have previously shown the dyad lysine to be a key player in binding to K^+ channels principally via electrostatic interactions between its positively charged extremity and carbonyl oxygen atoms of the channel selectivity filter [9,10,19]. It was thus hypothesized that the presence of an additional positive charge in a position adjacent to the putative dyad lysine (Fig. 5) could impair the electrostatic interactions necessary for toxin binding. Thus, mutants of κ-KTx1.3, with the lysine at position 20 mutated to a neutral (κ-KTx1.3 K20A) or another positively charged (κ-KTx1.3 K20R) amino acid or subjected to charge-reversal (κ-KTx1.3 K20E), were chemically synthesized for further electrophysiological characterization.

2.8. Functional characterization of κ-KTx1.3 mutants

The effects of the κ-KTx1.3 mutants on oocyte-expressed Kv 1.1, Kv 1.2 or Kv 1.3 channels were studied. The application of 200 μM of κ-KTx1.3 K20E produced 80.3 and 38.2% blockade of Kv 1.2 and Kv 1.3 channels, respectively, whereas only a small effect (10.7% blockade) was observed on Kv 1.1 channels (Fig. 6). The addition of 200 μM κ-KTx1.3 K20A resulted in a 44.6% blockade of Kv 1.1 channels as well as 35.0 and 44.1% blockade of Kv 1.2 and Kv 1.3 channels, respectively (Fig. 6). κ-KTx1.3 K20R did not produce any blockade of the three Kv 1 channels.

The blockade induced by κ-KTx1.3 K20A on Kv 1.1, Kv 1.2 and Kv 1.3 (Fig. 7A–C), and by κ-KTx1.3 K20E on Kv 1.2 and Kv 1.3 (Fig. 7D and 7E), were concentration-dependent. The IC_{50} values for κ-KTx1.3 K20A deter-

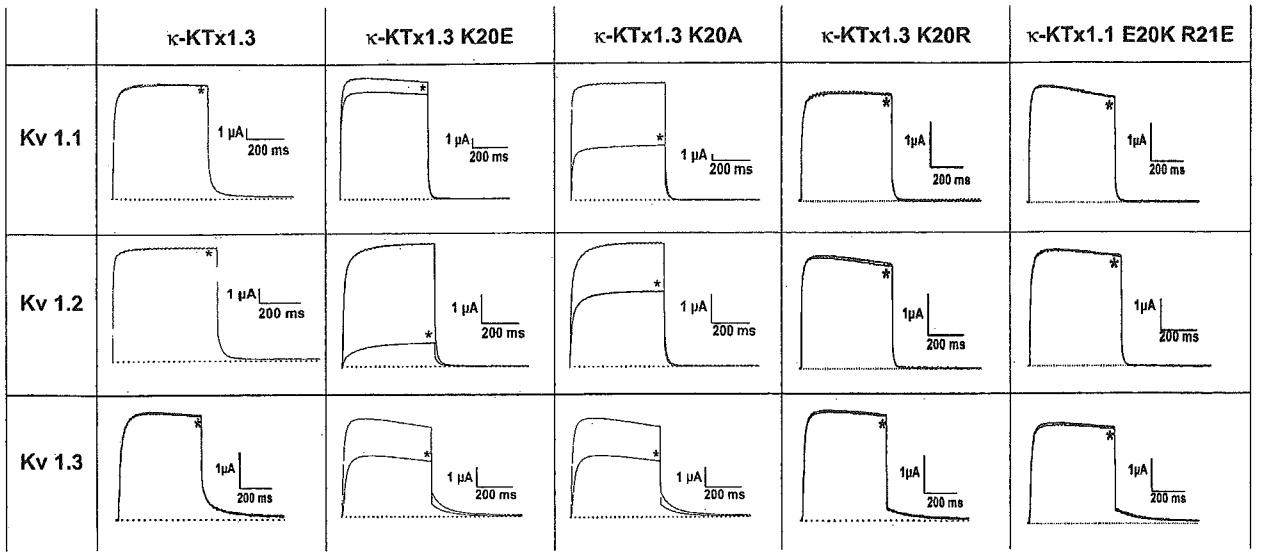

Fig. 6. Effects of κ-KTx1.3, κ-KTx1.3 K20E, κ-KTx1.3 K20A, κ-KTx1.3 K20R and the double mutant κ-KTx1.1 E20K R21E on Kv 1.1, Kv 1.2 and Kv 1.3 channels expressed in *X. laevis* oocytes. Current traces were evoked in oocytes expressing Kv channels by depolarizations to 0 mV from a holding potential of −90 mV and then clamped back to −50 mV. Asterisk (*) indicates the comparison of control condition to the presence of the toxin. After application of 200 μM of κ-KTx1.3 K20E, a small effect was observed on Kv 1.1 channels (10.7 ± 2.4% block) whereas 80.3 ± 6.9% and 38.2 ± 4.1% blockade were obtained on Kv 1.2 and Kv 1.3 channels, respectively. After application of 200 μM of κ-KTx1.3 K20A, we observed 44.6 ± 3.1% block on Kv 1.1 channels, 35.0 ± 3.8% on Kv 1.2 channels and 44.1 ± 4.2% block on Kv 1.3 channels. Native κ-KTx1.3 as well as κ-KTx1.3 K20R and κ-KTx1.1 E20K R21E did not produce any block of the Kv 1 channels tested. Data are the mean ± S.E.M. of at least four experiments.

mined by a sigmoidal fit were 110.7 ± 7.7 μM for Kv 1.1, 36.9 ± 4.9 μM for Kv 1.2 and 115.7 ± 7.3 μM for Kv 1.3 (Fig. 6F). The IC_{50} values for κ-KTx1.3 K20E were 36.8 ± 4.9 μM for Kv 1.2 and 53.7 ± 6.7 μM for Kv 1.3 (Fig. 6F). The block by both mutants was reversible upon washing-out and also shown to be voltage-independent (data not shown).

3. Discussion

Molecular models based on comparative analysis of the protein or peptide under investigation can pave the way for key experimental work to determine their biological activity more rapidly and in greater detail [20]. In this context, the significant structural homology between κ-KTx1.3 and κ-hefutoxin 1, including the presence of the functional dyad residues Y5 and K19 in identical positions, strongly suggested that the biological activity of κ-KTx1.3 would correspond to that of κ-hefutoxin 1. Previously, it was on the basis of the secondary structure of κ-hefutoxin 1, specifically the presence of the functional dyad (Y5, K19), that its K^+ channel blocking activity was predicted [13]. This was experimentally confirmed by the demonstration that κ-hefutoxin 1 produced concentration-dependent, voltage-independent and reversible blockade of currents through oocyte-expressed Kv 1.2 and Kv 1.3 channels with IC_{50} values of 40 and 150 μM, respectively [13]. Kv 1.1 channels were not significantly affected by κ-hefutoxin, suggesting that its affinity for Kv 1-type channels was Kv 1.2 > Kv 1.3 ⋙ Kv 1.1. Furthermore, mutational analysis identified Y5 and K19 as the key residues for bioactivity since their mutation to alanine, singly or together, resulted in a total loss of K^+ channel blockade [13].

Despite their unrelated structures and sources, toxins derived from animal venoms across different phyla, contain a key "dyad" composed of a positively charged residue (usually a lysine) and a hydrophobic residue (usually an aromatic amino acid) that constitute a minimal functional core for these toxins to bind to Kv 1 channels [8,13–15,21–23]. Additional residues may confer each toxin with a specific binding profile, the determination of subtype specificity for instance [21,24]. Interestingly, recent studies have also suggested that the functional dyad per se is not a prerequisite for toxin binding to Kv channels, in which case, other residues may act to form "multipoint interactions" with these channels [25–27].

This diverse array of toxins, however, all bind to a highly conserved region among K+ channels located at the pore helix and selectivity filter [9,10,15,22,27]. Generally, the binding of toxins to Kv 1 channels involves a combination of electrostatic, hydrophobic and hydrogen bonding interactions [27]. The major determinant of toxin binding to Kv 1 channels is likely to be the electrostatic interactions between the extremity of the dyad lysine, which protrudes into the ion-channel pore, and carbonyl oxygen atoms of residues from the highly conserved region of the channel selectivity filter [9,10,15,19,22,27,28]. Hydrophobic interactions between the dyad hydrophobic residue and aromatic residues protruding in the channel vestibule are believed to reinforce the critical electrostatic interaction

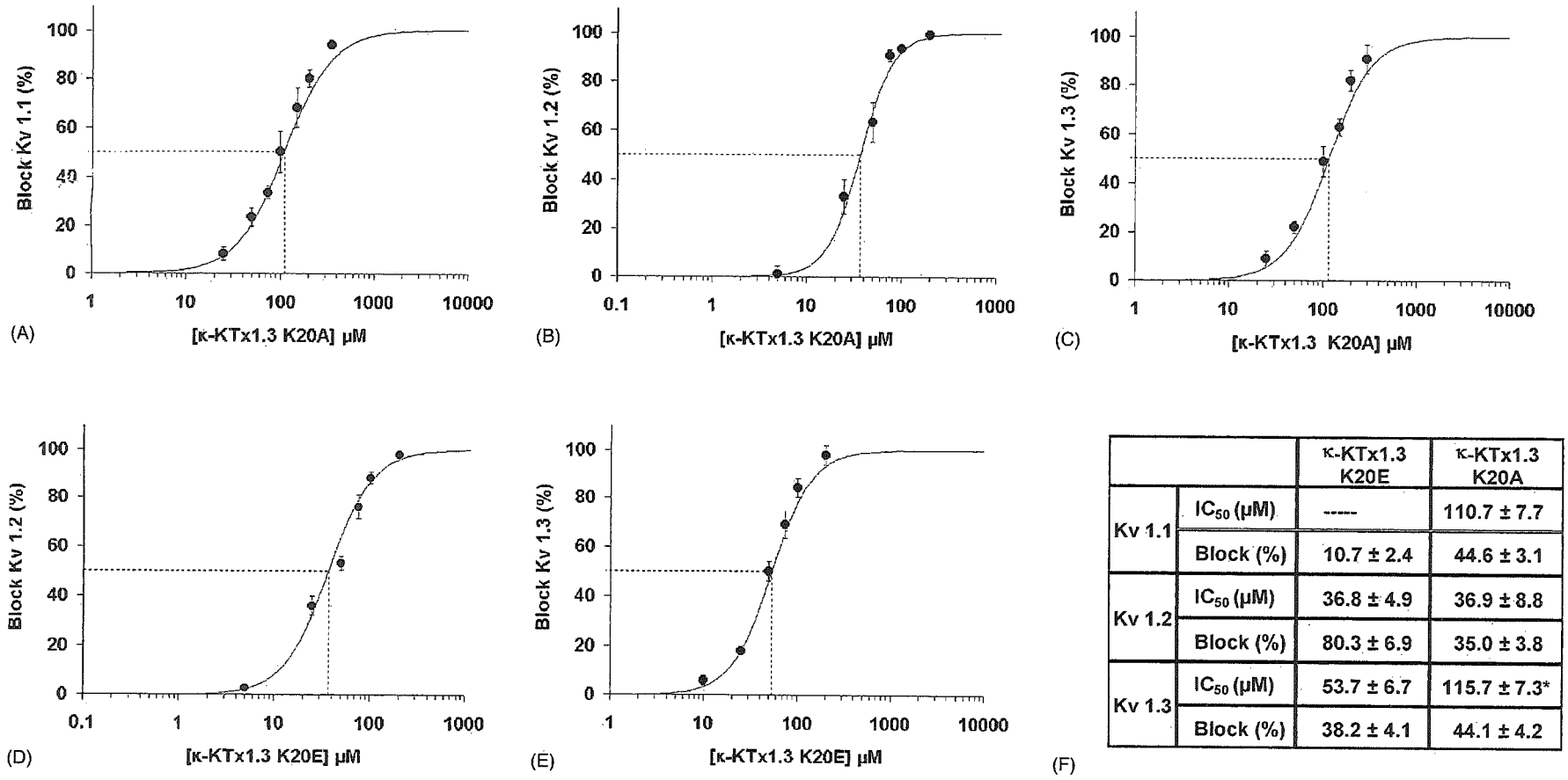

(F)

		κ-KTx1.3 K20E	κ-KTx1.3 K20A
Kv 1.1	IC_{50} (μM)	-----	110.7 ± 7.7
	Block (%)	10.7 ± 2.4	44.6 ± 3.1
Kv 1.2	IC_{50} (μM)	36.8 ± 4.9	36.9 ± 8.8
	Block (%)	80.3 ± 6.9	35.0 ± 3.8
Kv 1.3	IC_{50} (μM)	53.7 ± 6.7	115.7 ± 7.3*
	Block (%)	38.2 ± 4.1	44.1 ± 4.2

Fig. 7. Concentration dependence of the block induced by κ-KTx1.3 K20A on Kv 1.1, Kv 1.2 and Kv 1.3 (A–C) and κ-KTx1.3 K20E on Kv 1.2 and Kv 1.3 (D and E) channels. Currents were normalized as a function of the maximal block percentage set at 100%. Currents were evoked by a depolarization to 0 mV from a holding potential of −90 mV. The IC_{50} values and the maximal percentage block are shown (F). Data are the mean ± S.E.M. of at least four experiments at each concentration. $^{*}p < 0.05$, statistically significant when compared to κ-KTx1.3K20E.

by surrounding the lysine side-chain and allowing its exclusion from solvent [22]. Thus, it appears that the conserved functional dyad residues from scorpion toxins bind via conserved molecular interactions to Kv 1 channels.

However, on screening κ-KTx1.3 for K^+ channel blocking activity on oocyte-expressed Kv 1-type channels, it was found that the toxin did not show the expected electrophysiological effects even at concentrations as high as 1 mM. On analyzing the primary structure of κ-KTx1.3, it was hypothesized that the presence of an additional positively charged residue (K20) that was found flanking the putative key lysine (K19) in its primary sequence could hinder the proposed electrostatic interaction of κ-KTx1.3 with the K^+ channel. Interestingly, the single mutation of K20 in κ-KTx1.3 to a negatively charged glutamic acid, as found in κ-hefutoxin 1, resulted in the mutant κ-KTx1.3 K20E acquiring biological activity almost identical to that of κ-hefutoxin 1 with respect to subtype selectivity and affinity. Accordingly, κ-KTx1.3 K20E produced blockade of Kv 1.2 (IC_{50} ~37 μM) and Kv 1.3 (IC_{50} ~54 μM) but not Kv 1.1 channels. In contrast, the mutant κ-KTx1.3 K20A produced blockade of both Kv 1.2 (IC_{50} ~37 μM) and Kv 1.3 (IC_{50} ~116 μM) and in addition, also acquired affinity for Kv 1.1 channels (IC_{50} ~111 μM). Although, both κ-hefutoxin 1 and the κ-KTx1.3 mutants produced partial blockade of Kv 1 channels, such partial blocks of these channels have also been reported before for several scorpion toxins, possibly due to imperfect ion channel pore occlusion [28–30]. To provide conclusive evidence of our hypothesis, two other mutants were synthesized: κ-KTx1.3 K20R, wherein lysine 20 was mutated to arginine, and κ-KTx1.1 E20K R21E, a double mutant of κ-hefutoxin 1, with the residues at positions 20 and 21 mutated to lysine and glutamic acid, respectively, as found in κ-KTx1.3. Both caused no significant block on the three Kv channels.

These data suggest that the presence of an additional positive charge in a position adjacent to the dyad lysine in κ-KTx1.3 is sufficient, presumably by electrostatic repulsion, to prevent its ability to produce functional blockade of Kv 1.2 and Kv 1.3 channels. On the other hand, the functional blockade of Kv 1.1 channels by κ-KTx1.3 was impeded if the dyad lysine was flanked by either a positively or negatively charged amino acid. Together, these data support previous reports [13–15,22–24] that Kv 1 channel toxins establish high affinity interactions principally or in part via electrostatic interactions involving the key dyad lysine and in addition suggest that the toxin-induced functional blockade of Kv 1 channels may be easily compromised by changes in the charge environment of the dyad region.

While the κ-KTx subfamily of scorpion toxins, which interact only weakly with Kv 1 channel subtypes, are yet to be investigated for biological activity against other K^+ channels, it must also be remembered that despite the remarkable achievements made in the recent past with respect to the biology of K^+ channels, many K^+ channel currents remain elusive and await the discovery of novel ligands for their identification and characterization [10,12]. Hence it is possible that scorpion toxins such as κ-hefutoxin 1 and κ-KTx1.3 may have been selected by natural evolution for other high-affinity molecular targets that are still currently unknown.

Acknowledgements

K.S. was supported by a grant-in-aid from the Ministry of Education, Science, Sports, Culture and Technology of Japan. S.N. was the recipient of a research scholarship from the National University of Singapore.

References

[1] Gwee MCE, Nirthanan S, Khoo HE, Gopalakrishnakone P, Kini RM, Cheah LS. Autonomic effects of some scorpion venoms and toxins. Clin Exp Pharmacol Physiol 2002;29:795–801.
[2] Martin-Euclaire M-F. Neurotoxins from scorpion venoms. In: Massaro EJ, editor. Handbook of neurotoxicology, vol. 1. Totowa, NJ: Humana; 2001. p. 503–8.
[3] Olamendi-Portugal T, Gomez-Lagunas F, Gurrola GB, Possani LD. A novel structural class of K^+ channel blocking toxin from the scorpion *Pandinus imperator*. Biochem J 1996;315:977–81.
[4] Kharrat R, Mansuelle P, Sampieri F, Crest M, Oughideni R, Van Rietschoten J. Maurotoxin, a four disulfide bridge toxin from *Scorpio maurus* venom: purification, structure and action on potassium channels. FEBS Lett 1997;406:284–90.
[5] Lebrun B, Romi-Lebrun R, Martin-Eauclaire MF, Yasuda A, Ishiguro M, Oyama Y, et al. A four-disulphide toxin, with high affinity towards voltage-gated K+ channels, isolated from *Heterometrus spinifer* (Scorpionidae) venom. Biochem J 1997;328:321–7.
[6] Strong PN. Potassium channel toxins. Pharmacol Ther 1990;46:137–62.
[7] Possani LD, Merino E, Corona M, Becerril B. Scorpion genes and peptides specific for potassium channels: structure, function and evolution. In: Menez A, editor. Perspectives in molecular toxinology. Chichester, England: John Wiley & Sons; 2002. p. 201–11.
[8] Darbon H, Blanc E, Sabatier J-M. Three-dimensional structure of scorpion toxins: towards a new model of interaction with potassium channels. Perspect Drug Discov Des 1999;15/16:41–60.
[9] Garcia ML, Gao Y, McManus OB, Kaczorowski GJ. Potassium channels: from scorpion venoms to high-resolution structure. Toxicon 2001;39:739–48.
[10] Rodriguez de la Vega RC, Merino E, Becerril B, Possani LD. Novel interactions between K^+ channels and scorpion toxins. Trends Pharmacol Sci 2003;24:222–7.
[11] Tytgat J, Chandy KG, Garcia ML, Gutman GA, Martin-Euclaire M-F, Walt JJ, et al. A unified nomenclature for short-chain peptides isolated from scorpion venoms: α-KTx molecular subfamilies. Trends Pharmacol Sci 1999;20:444–7.
[12] Possani LD, Selisko B, Gurrola GB. Structure and function of scorpion toxins affecting K+-channels. Perspect Drug Discov Des 1999;15/16:15–40.
[13] Srinivasan KN, Sivaraja V, Huys I, Sasaki T, Cheng B, Kumar TKS, et al. κ-Hefutoxin 1, a novel toxin from *Heterometrus fulvipes* with unique structure and function. Importance of the functional dyad in potassium channel selectivity. J Biol Chem 2002;277:30040–7.
[14] Dauplais M, Lecoq A, Song J, Cotton J, Jamin N, Gilquin B, et al. On the convergent evolution of animal toxins. Conservation of a dyad of functional residues in potassium channel-blocking toxins with unrelated structures. J Biol Chem 1997;272:4302–9.

[15] Menez A, Servent D, Gasparini S. The binding sites of animal toxins involve two components: a clue for selectivity, evolution and design of proteins? In: Menez A, editor. Perspectives in molecular toxinology. Chichester, England: John Wiley & Sons; 2002. p. 175–200.
[16] Nirthanan S, Joseph JS, Gopalakrishnakone P, Khoo HE, Cheah LS, Gwee MC... Biochemical and pharmacological characterization of the venom of the black scorpion (*Heterometrus spinifer*). Biochem Pharmacol 2002;63:49–55.
[17] Srinivasan KN, Nirthanan S, Sasaki T, Sato K, Cheng B, Gwee MCE, et al. Functional site of bukatoxin, a K-type sodium channel neurotoxin from the Chinese scorpion (*Buthus Martensi* Karsch) venom: probable role of the 52 PDKVP 56 loop. FEBS Lett 2001;494:145–9.
[18] Liman ER, Tytgat J, Hess P. Subunit stoichiometry of a mammalian K^+ channel determined by construction of multimeric cDNAs. Neuron 1992;9:861–71.
[19] Miller C. The charybdotoxin family of K^+ channel-blocking peptides. Neuron 1995;15:5–10.
[20] Possani LD, Rodriguez de la Vega RC. Response to Xu et al.: Hypothesis-driven science paves the way for new discoveries. Trends Pharmacol Sci 2003;24:448–9.
[21] Gasparini S, Danse J-M, Lecoq A, Pinkasfeld S, Zinn-Justin S, Young LC, et al. Delineation of the functional site of α-dendrotoxin. The functional topographies of dendrotoxins are different but share a conserved core with those of other Kv 1 potassium channel-blocking toxins. J Biol Chem 1998;273:25393–403.
[22] Gilquin B, Racape J, Wrisch A, Visan V, Lecoq A, Grissmer S, et al. Structure of the BgK-Kv 1.1 complex based on distance restraints identified by double mutant cycles. Molecular basis for convergent evolution of Kv 1 channel blockers. J Biol Chem 2002;277:37406–13.
[23] Huys I, Tytgat J. Evidence for a function-specific mutation in the neurotoxin, parabutoxin 3. Eur J Neurosci 2003;17:1786–92.
[24] Alessandri-Haber N, Lecoq A, Gasparini S, Grangier-Macmath G, Jacquet G, Harvey AL, et al. Mapping the functional anatomy of BgK on Kv 1.1, Kv 1. 2 and Kv 1. 3. Clues to design analogs with enhanced selectivity. J Biol Chem 1999;274:35653–61.
[25] Batista CV, Gomez-Lagunas F, Rodriguez de la Vega RC, Hajdu P, Panyi G, Gaspar R, et al. Two novel toxins from the Amazonian scorpion *Tityus cambridgei* that block Kv 1.3 and *Shaker* B K^+ channels with distinctly different affinities. Biochem Biophys Acta 2002;1601:123–31.
[26] Mouhat S, Mosbah A, Visan V, Wulff H, Delepierre M, Darbon H, et al. The "functional" dyad of scorpion toxin Pi1 is not itself a prerequisite for toxin binding to the voltage-gated Kv 1.2 potassium channels. Biochem J 2004;377:25–36.
[27] Xu C-Q, Zhu S-Y, Chi C-W, Tytgat J. Turret and pore block of K^+ channels: what is the difference?. Trends Pharmacol Sci 2003;24: 446–68.
[28] M'Barek S, Mosbah A, Sandoz G, Fajloun Z, Olamendi-Portugal T, Rochat H, et al. Synthesis and characterization of Pi4, a scorpion toxin from *Pandinus imperator* that acts on K^+ channels. Eur J Biochem 2003;270:3583–92.
[29] Fajloun Z, Carlier E, Lecomte C, Geib S, Di Luccio E, Bichet D, et al. Chemical synthesis and characterization of Pi1, a scorpion toxin from *Pandinus imperator* active on K^+ channels. Eur J Biochem 2000;267:5149–55.
[30] Huys I, Dyason K, Waelkens E, Verdonck F, van Zyl J, du Plessis J, et al. Purification, characterization and biosynthesis of parabutoxin 3, a component of *Parabuthus transvaalicus* venom. Eur J Biochem 2002;269:1854–65.

J|A|C|S
ARTICLES
Published on Web 06/29/2005

Selective Zinc Sensor Molecules with Various Affinities for Zn^{2+}, Revealing Dynamics and Regional Distribution of Synaptically Released Zn^{2+} in Hippocampal Slices

Kensuke Komatsu,† Kazuya Kikuchi,*,†,‡ Hirotatsu Kojima,† Yasuteru Urano,†,‡ and Tetsuo Nagano*,†

Contribution from the Graduate School of Pharmaceutical Sciences, The University of Tokyo, 7-3-1 Hongo, Bunkyo-ku, Tokyo 113-0033, Japan, and Presto, JST Agency, Honcho, Kawaguchi-shi, Saitama 332-0012, Japan

Received January 17, 2005; E-mail: tlong@mol.f.u-tokyo.ac.jp; kkikuchi@mol.f.u-tokyo.ac.jp

Abstract: We have developed a series of fluorescent Zn^{2+} sensor molecules with distinct affinities for Zn^{2+}, because biological Zn^{2+} concentrations vary over a wide range from sub-nanomolar to millimolar. The new sensors have K_d values in the range of 10^{-8}–10^{-4} M, compared with 2.7 nM for ZnAF-2. They do not fluoresce in the presence of other biologically important metal ions such as calcium or magnesium, and they can detect Zn^{2+} within 100 ms. In cultured cells, the fluorescence intensity of ZnAF-2 was saturated at low Zn^{2+} concentration, while that of ZnAF-3 (K_d = 0.79 μM) was not saturated even at relatively high Zn^{2+} concentrations. In hippocampal slices, we measured synaptic release of Zn^{2+} in response to high-potassium-induced depolarization. ZnAF-2 showed similar levels of fluorescence increase in dentate gyrus (DG), CA3 and CA1, which were indistinguishable. However, ZnAF-3 showed a fluorescence increase only in DG. Thus, by using a combination of sensor molecules, it was demonstrated for the first time that a higher Zn^{2+} concentration is released in DG than in CA3 or CA1 and that we can easily visualize Zn^{2+} concentration over a wide range. We believe that the use of various combinations of ZnAF family members will offer unprecedented versatility for fluorescence-microscopic imaging of Zn^{2+} in biological applications.

Introduction

For over a century, zinc (Zn^{2+}) has been known as an essential trace element, acting as a structural component of proteins or in the catalytic site of enzymes.[1] In general, Zn^{2+} is tightly associated with proteins and peptides. However, recent advances in cell biology have revealed a fraction of Zn^{2+} that is free or chelatable in some organs (brain,[2] pancreas,[3] and spermatozoa[4]). In the brain, a considerable amount of chelatable Zn^{2+} is sequestered in the vesicles of presynaptic neurons and is released when the neurons are active.[5] Zn^{2+} is also associated with neuronal disorders,[6] though its role in them is poorly understood. So there is much interest in its detection in vivo, where its concentration varies from 10^{-10} M in the cytoplasm[7] to 10^{-4} M in some vesicles.[8] However, the lack of appropriate detecting tools, especially for such a broad concentration range, hinders further investigation of this spectroscopically silent metal ion.

Fluorescent sensor molecules offer useful information about chelatable Zn^{2+} in cellular systems, because we can study the concentration or distribution of Zn^{2+} in real time,[9] and fluorescence imaging of Zn^{2+} has become a widely and frequently used technique. The first reported sensor molecules for cellular Zn^{2+} were arenesulfonamides of 8-aminoquinoline, such as TSQ [10] and Zinquin.[11] They form 1:2 complexes with Zn^{2+}, emitting strong fluorescence on UV excitation. Since then, various kinds of fluorescent Zn^{2+} sensor molecules have been developed and examined, such as TSQ derivatives,[12] peptide or protein-based sensors,[13] sensors for ratiometric measurement,[14] and others.[15] Above all, various fluorescein derivatives were introduced: NGs,[16] ZPs,[17] FluoZins,[18] ZnAFs,[19] and others.[20] Fluorescein derivatives have many advantages over

† The University of Tokyo.
‡ JST Agency.

(1) (a) Vallee, B. L.; Falchuk, K. H. *Physiol. Rev.* **1993**, *73*, 79–118. (b) Berg, J. M.; Shi, Y. G. *Science* **1996**, *271*, 1081–1085.
(2) (a) Frederickson, C. J. *Int. Rev. Neurobiol.* **1989**, *31*, 145–238. (b) Frederickson, C. J.; Bush, A. I. *Biometals* **2001**, *14*, 353–366. (c) Li, Y.; Hough, C.; Sarvey, J. *Sci. STKE* **2003**, *182*, 19.
(3) (a) Zalewski, P. D.; Millard, S. H.; Forbes, I. J.; Kapaniris, O.; Slavotinek, A.; Betts, W. H.; Ward, A. D.; Lincoln, S. F.; Mahadevan, I. *J. Histochem. Cytochem.* **1994**, *42*, 877–884. (b) Qian, W. J.; Gee, K. R.; Kennedy, R. T. *Anal. Chem.* **2003**, *75*, 3468–3475.
(4) Zalewski, P. D.; Jian, X.; Soon, L. L. L.; Breed, W. G.; Seamark, R. F.; Lincoln, S. F.; Ward, A. D.; Sun, F. Z. *Reprod., Fertil. Dev.* **1996**, *8*, 1097–1105.
(5) (a) Assaf, S. Y.; Chung, S. H. *Nature* **1984**, *308*, 734–736. (b) Howell, G. A.; Welch, M. G.; Frederickson, C. J. *Nature* **1984**, *308*, 736–738.
(6) Bush, A. I. *Curr. Opin. Chem. Biol.* **2000**, *4*, 184–191.
(7) (a) Canzoniero, L. M. T.; Sensi, S. L.; Choi, D. W. *Neurobiol. Dis.* **1997**, *4*, 275–279. (b) Outten, C. E.; O'Halloran, T. V. *Science* **2001**, *292*, 2488–2492. (c) Thompson, R. B.; Peterson, D.; Mahoney, W.; Cramer, M.; Maliwal, B. P.; Suh, S. W.; Frederickson, C.; Fierke, C.; Herman, P. *J. Neurosci. Methods* **2002**, *118*, 63–75. (d) Finney, L. A.; O'Halloran, T. V. *Science* **2003**, *300*, 931–936.
(8) Frederickson, C. J.; Klitenick, M. A.; Manton, W. I.; Kirkpatrick, J. B. *Brain Res.* **1983**, *273*, 335–339.
(9) Mason, W. T. *Fluorescent and Luminescent Probes for Biological Activity*; 2nd ed.; Academic Press: New York, 1999.
(10) Frederickson, C. J.; Kasarskis, E. J.; Ringo, D.; Frederickson, R. E. *J. Neurosci. Methods* **1987**, *20*, 91–103.
(11) Zalewski, P. D.; Forbes, I. J.; Betts, W. H. *Biochem. J.* **1993**, *296*, 403–408.

10.1021/ja050301e CCC: $30.25

Zinquin. The high quantum yield in aqueous solution provides high sensitivity in the cellular environment, and the excitation wavelength in the visible range minimizes cell damage during irradiation. These sensors have led to great advances in Zn^{2+} biology, and further development of sensor molecules would be very valuable.[21]

We set out several criteria for developing novel fluorescent Zn^{2+} sensor molecules. First, for intensity-based measurement, the sensor should have no signal in the absence of Zn^{2+}, and the signal should increase in the presence of Zn^{2+} in an all-or-none fashion. Second, the sensor should be selective for Zn^{2+}, without interference by biologically important metal ions, such as Ca^{2+} or Mg^{2+}. Third, complexation and decomplexation with Zn^{2+} should be rapid, to provide a fast response. Fourth, for intracellular study, the sensor should be derivatizable into a cell-permeable form that can penetrate through the cell membrane and be hydrolyzed intracellularly to afford the sensor, which is then trapped in the cell. Fifth, their affinity for Zn^{2+} should be appropriate for the Zn^{2+} concentration range of interest.

We previously showed that ZnAFs, which satisfy most of the requirements mentioned above, can serve as useful tools for biological applications.[19,22] However, the affinity for Zn^{2+} remains an issue. To follow changes of Zn^{2+} concentration, it is desirable to use a sensor molecule whose apparent dissociation constant (K_d) is near the target concentration of Zn^{2+}. Almost all Zn^{2+} sensor molecules recently developed have K_d values in the nanomolar region (ZnAF-2, 2.7 nM), because cytosolic free Zn^{2+} concentration is controlled at ~1 nM or lower.[7] Neither Zn^{2+} deficiency nor Zn^{2+} excess affects cell viability and function,[23] and these sensors can easily be used in cytoplasm, etc. However, at higher concentrations of Zn^{2+}, the fluorescence intensity of these sensors would be saturated. Zn^{2+} is known to be sequestered in synaptic vesicles of many excitatory forebrain neurons, and the concentration of Zn^{2+} inside the vesicle was reported to be in the micro- to millimolar range.[8] This vesicular Zn^{2+} is also released into synaptic space, where it is estimated to achieve peak levels of 10−30 μM.[24] In such circumstances, sensor molecules with high affinity would have no ability to detect changes of Zn^{2+} concentration. So, for precise analysis of the biological roles of Zn^{2+}, we require a range of sensor molecules with K_d values not only in the nM range, but also higher.

Among Zn^{2+} sensor molecules so far reported, only Newport Green ($K_d \sim 1$ μM) has been used as a low-affinity Zn^{2+} sensor to detect synaptically released Zn^{2+}, for which purpose the Zn^{2+} concentration was calculated on the basis of the K_d value.[24] There is little other evidence to support the idea that the release of Zn^{2+} reaches micromolar levels, so confirmation remains desirable.

Our purpose in this study is to develop a range of low-affinity sensor molecules whose K_d values are higher than nanomolar order without any loss of favorable characteristics, such as low basal fluorescence and selectivity for Zn^{2+}.

In designing low-affinity sensor molecules, we chose ZnAF-2 as a basal structure. ZnAF-2 has a fluorescein fluorophore conjugated to *N*,*N*-bis(2-pyridylmethyl)ethylenediamine as a Zn^{2+} chelator. The design of the chelator was based on the structure of TPEN (*N*,*N*,*N*′,*N*′-tetrakis(2-pyridylmethyl)ethylenediamine). These groups offer the following advantages. Derivatives of fluorescein that are amino-substituted at the benzoic acid moiety emit little fluorescence due to the photo-induced electron transfer (PeT) quenching pathway, resulting in low basal fluorescence and high sensitivity.[20a] TPEN is known as a selective chelator of Zn^{2+} over Ca^{2+} or Mg^{2+}.[25] For intracellular application, a cell-permeant form can be obtained readily, because the TPEN moiety itself cannot be protonated at physiological pH, so the sensor remains intact. Moreover, the structural separation of sensor and chelator moieties means that modification of the chelator should not affect the fluorescence properties, such as maximum/minimum quantum yield or excitation/emission wavelength. This approach, leaving the fluorophore intact, is a characteristic advantage of fluorescent sensors utilizing the PeT mechanism. Therefore, we set out to develop a series of Zn^{2+} sensor molecules by modification of

(12) (a) Budde, T.; Minta, A.; White, J. A.; Kay, A. R. *Neuroscience* **1997**, *79*, 347−358. (b) Nasir, M. S.; Fahrni, C. J.; Suhy, D. A.; Kolodsick, K. J.; Singer, C. P.; O'Halloran, T. V. *J. Biol. Inorg. Chem.* **1999**, *4*, 775−783. (c) Fahrni, C. J.; O'Halloran, T. V. *J. Am. Chem. Soc.* **1999**, *121*, 11448−11458. (d) Kimber, M. C.; Mahadevan, I. B.; Lincoln, S. F.; Ward, A. D.; Betts, W. H. *Aust. J. Chem.* **2001**, *54*, 43−49. (e) Pearce, D. A.; Jotterand, N.; Carrico, I. S.; Imperiali, B. *J. Am. Chem. Soc.* **2001**, *123*, 5160−5161. (f) Hendrickson, K. M.; Geue, J. P.; Wyness, O.; Lincoln, S. F.; Ward, A. D. *J. Am. Chem. Soc.* **2003**, *125*, 3889−3895.

(13) (a) Walkup, G. K.; Imperiali, B. *J. Am. Chem. Soc.* **1996**, *118*, 3053−3054. (b) Walkup, G. K.; Imperiali, B. *J. Am. Chem. Soc.* **1997**, *119*, 3443−3450. (c) Walkup, G. K.; Imperiali, B. *J. Org. Chem.* **1998**, *63*, 6727−6731. (d) Thompson, R. B.; Maliwal, B. P.; Fierke, C. A. *Anal. Chem.* **1998**, *70*, 1749−1754. (e) Barondeau, D. P.; Kassmann, C. J.; Tainer, J. A.; Getzoff, E. D. *J. Am. Chem. Soc.* **2002**, *124*, 3522−3524. (f) Hong, S. H.; Maret, W. *Proc. Natl. Acad. Sci. U.S.A.* **2003**, *100*, 2255−2260. (g) Shults, M. D.; Pearce, D. A.; Imperiali, B. *J. Am. Chem. Soc.* **2003**, *125*, 10591−10597.

(14) (a) Maruyama, S.; Kikuchi, K.; Hirano, T.; Urano, Y.; Nagano, T. *J. Am. Chem. Soc.* **2002**, *124*, 10650−10651. (b) Henary, M. M.; Fahrni, C. J. *J. Phys. Chem. A* **2002**, *106*, 5210−5220. (c) Taki, M.; Wolford, J. L.; O'Halloran, T. V. *J. Am. Chem. Soc.* **2004**, *126*, 712−713. (d) Henary, M. M.; Wu, Y. G.; Fahrni, C. I. *Che.−Eur. J.* **2004**, *10*, 3015−3025.

(15) (a) Hanaoka, K.; Kikuchi, K.; Kojima, H.; Urano, Y.; Nagano, T. *Angew. Chem., Int. Ed.* **2003**, *42*, 2996−2999. (b) Hanaoka, K.; Kikuchi, K.; Kojima, H.; Urano, Y.; Nagano, T. *J. Am. Chem. Soc.* **2004**, *126*, 12470−12476. (c) Lim, N. C.; Yao, L.; Freake, H. C.; Bruckner, C. *Bioorg. Med. Chem. Lett.* **2003**, *13*, 2251−2254. (d) Koutaka, H.; Kosuge, J.; Fukasaku, N.; Hirano, T.; Kikuchi, K.; Urano, Y.; Kojima, H.; Nagano, T. *Chem. Pharm. Bull.* **2004**, *52*, 700−703.

(16) Haugland, R. P. *Handbook of Fluorescent Probes and Research Products*; 8th ed.; Molecular Probes, Inc.: Eugene, OR, 2001.

(17) (a) Walkup, G. K.; Burdette, S. C.; Lippard, S. J.; Tsien, R. Y. *J. Am. Chem. Soc.* **2000**, *122*, 5644−5645. (b) Burdette, S. C.; Walkup, G. K.; Spingler, B.; Tsien, R. Y.; Lippard, S. J. *J. Am. Chem. Soc.* **2001**, *123*, 7831−7841. (c) Burdette, S. C.; Frederickson, C. J.; Bu, W. M.; Lippard, S. J. *J. Am. Chem. Soc.* **2003**, *125*, 1778−1787. (d) Nolan, E. M.; Burdette, S. C.; Harvey, J. H.; Hilderbrand, S. A.; Lippard, S. J. *Inorg. Chem.* **2004**, *43*, 2624−2635. (e) Chang, C. J.; Nolan, E. M.; Jaworski, J.; Burdette, S. C.; Sheng, M.; Lippard, S. J. *Chem. Biol.* **2004**, *11*, 203−210. (f) Chang, C. J.; Nolan, E. M.; Jaworski, J.; Okamoto, K. I.; Hayashi, Y.; Sheng, M.; Lippard, S. J. *Inorg. Chem.* **2004**, *43*, 6774−6779.

(18) (a) Gee, K. R.; Zhou, Z. L.; Ton-That, D.; Sensi, S. L.; Weiss, J. H. *Cell Calcium* **2002**, *31*, 245−251. (b)Gee, K. R.; Zhou, Z. L.; Qian, W. J.; Kennedy, R. *J. Am. Chem. Soc.* **2002**, *124*, 776−778.

(19) (a) Hirano, T.; Kikuchi, K.; Urano, Y.; Higuchi, T.; Nagano, T. *J. Am. Chem. Soc.* **2000**, *122*, 12399−12400. (b) Hirano, T.; Kikuchi, K.; Urano, Y.; Nagano, T. *J. Am. Chem. Soc.* **2002**, *124*, 6555−6562.

(20) (a) Hirano, T.; Kikuchi, K.; Urano, Y.; Higuchi, T.; Nagano, T. *Angew. Chem.-Int. Edit.* **2000**, *39*, 1052−1054. (b) Sensi, S. L.; Ton-That, D.; Weiss, J. H.; Rothe, A.; Gee, K. R. *Cell Calcium* **2003**, *34*, 281−284. (c) Chang, C. J.; Jaworski, J.; Nolan, E. M.; Sheng, M.; Lippard, S. J. *Proc. Natl. Acad. Sci. U.S.A.* **2004**, *101*, 1129−1134.

(21) (a) Frederickson, C. *Sci. STKE* **2003**, *182*, 18. (b) Jiang, P. J.; Guo, Z. J. *Coord. Chem. Rev.* **2004**, *248*, 205−229. (c) Kikuchi, K.; Komatsu, K.; Nagano, T. *Curr. Opin. Chem. Biol.* **2004**, *8*, 182−191.

(22) Ueno, S.; Tsukamoto, M.; Hirano, T.; Kikuchi, K.; Yamada, M. K.; Nishiyama, N.; Nagano, T.; Matsuki, N.; Ikegaya, Y. *J. Cell Biol.* **2002**, *158*, 215−220.

(23) (a) MacDiarmid, C. W.; Milanick, M. A.; Eide, D. J. *J. Biol. Chem.* **2003**, *278*, 15065−15072. (b) Colvin, R. A.; Fontaine, C. P.; Laskowski, M.; Thomas, D. *Eur. J. Pharmacol.* **2003**, *479*, 171−185.

(24) (a) Li, Y.; Hough, C. J.; Suh, S. W.; Sarvey, J. M.; Frederickson, C. J. *J. Neurophysiol.* **2001**, *86*, 2597−2604. (b) Li, Y.; Hough, C. J.; Frederickson, C. J.; Sarvey, J. M. *J. Neurosci.* **2001**, *21*, 8015−8025.

(25) Arslan, P.; Divirgilio, F.; Beltrame, M.; Tsien, R. Y.; Pozzan, T. *J. Biol. Chem.* **1985**, *260*, 2719−2727.

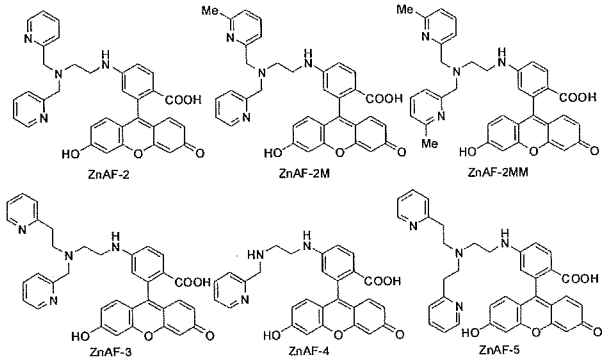

Figure 1. Structures of ZnAF family members. ZnAF-2 was previously reported to visualize Zn^{2+} in brain slices. The other sensor molecules were newly synthesized.

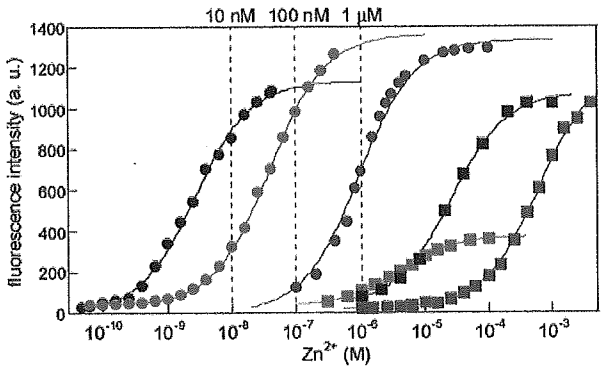

Figure 2. Changes of fluorescence intensity for 1 μM ZnAFs (ZnAF-2, black circle; ZnAF-2M, red circle; ZnAF-2MM, red square; ZnAF-3, blue circle; ZnAF-4, black square; and ZnAF-5, blue square) as a function of the concentration of free Zn^{2+} in 100 mM HEPES buffer (pH 7.4, $I = 0.1$ ($NaNO_3$)).

the TPEN moiety to obtain various K_d values without affecting the selectivity against other ions.

Here, we report a series of fluorescent sensor molecules for Zn^{2+} with various K_d values from nanomolar up to millimolar range. Their design, synthesis, and fluorescence properties are described. We also present applications to cultured cells and hippocampal slices.

Results and Discussion

Design and Synthesis. Figure 1 illustrates the structures of Zn^{2+} sensor molecules, ZnAF-2 and its new derivatives. ZnAF-2 was synthesized by conjugating 5-aminofluorescein and dipicolylamine via a linker, dibromoethane, so we introduced various chelators instead of dipicolylamine and left the fluorophore unchanged. The design was based on three strategies. First, we introduced steric hindrance at the nitrogen atom on the pyridine ring by substituting a methyl group at the 6-position (ZnAF-2M, ZnAF-2MM). Second, we removed one ligand, picolylamine (ZnAF-4). Last, we increased the distance between the ligands (ZnAF-3, ZnAF-5). The synthetic schemes for these sensors are described in the Supporting Information.

Fluorescence Properties. We measured the fluorescence intensity of these sensor molecules in various concentrations of Zn^{2+}. As we had expected, these sensors showed changes in fluorescence intensity at higher Zn^{2+} concentrations than ZnAF-2 (Figure 2) but retained almost the same fluorescence properties, such as absorption/emission wavelength and maximum/minimum quantum yield, which is convenient when using and comparing several sensors (Table 1). In each case, the fluorescence increase fitted well with a 1:1 binding model and the Hill coefficient of 1 suggests that a 1:1 Zn^{2+}–ZnAF complex was formed. The apparent dissociation constants were as follows: ZnAF-2M, 38 nM; ZnAF-2MM, 3.9 μM; ZnAF-3, 0.79 μM; ZnAF-4, 25 μM; and ZnAF-5, 0.60 mM (Table 2). Thus, we can follow a wide Zn^{2+} concentration range from 10^{-10} M up to 10^{-3} M by using different sensor molecules. Furthermore, by using them in combination, we can easily estimate the Zn^{2+} concentration. For example, if the concentration of free Zn^{2+} is 10 nM, there is strong fluorescence in ZnAF-2, weak fluorescence in ZnAF-2M, and no fluorescence in ZnAF-3 (Figure 2). At 100 nM Zn^{2+}, there is strong fluorescence in both ZnAF-2 and ZnAF-2M and little or no fluorescence in ZnAF-3. At 1 μM Zn^{2+}, there is strong fluorescence in ZnAF-3 and no fluorescence in ZnAF-4.

Among these sensors, ZnAF-2MM has lower quantum yield and fluorescence intensity in the presence of Zn^{2+} than the others. The fluorescence enhancement of ZnAFs, we consider, is attained through Zn^{2+} coordination to the amine on the benzoic acid moiety of fluorescein. In the absence of Zn^{2+}, the fluorescence is quenched due to the PeT from the benzoic acid moiety to the xanthene moiety. However, Zn^{2+} coordination alters the HOMO energy level of the benzoic acid moiety, thereby preventing PeT and leading to the enhancement of fluorescence from the xanthene moiety (fluorophore).[26] In ZnAF-2MM, the two methyl groups may alter the coordination structure of the Zn^{2+}–ZnAF complex, in a way that less strongly affects the HOMO energy level of the benzoic acid moiety, resulting in weak fluorescence.

Thus, we have completed developing a range of Zn^{2+} sensor molecules with various affinities for Zn^{2+} but whose fluorescence properties resemble those of ZnAF-2.

Determination of Complexing Rate. We then measured the complexing rate of these sensor molecules (Figure 3). When an excess amount of Zn^{2+} was added, all the sensors synthesized showed very rapid saturation of the fluorescence signal within about 100 ms, except for ZnAF-2MM, which reached maximum fluorescence after 1 s. Therefore, these sensors except for ZnAF-2MM are suitable for detecting rapid change in cellular Zn^{2+} concentration. The calculated association (k_{on}) and dissociation (k_{off}) constants are shown in Table 2. The k_{on} values of ZnAF-2M, ZnAF-3, and ZnAF-4 are almost the same as that of ZnAF-2, and the k_{off} values are larger than that of ZnAF-2, implying that these sensors can detect Zn^{2+} increase as fast as ZnAF-2 and Zn^{2+} decrease faster than ZnAF-2. ZnAF-2MM and ZnAF-5 have smaller k_{on} values than ZnAF-2. Apparently, just one picolyl group is important for the sensor to make a rapid complex with Zn^{2+}. On the other hand, the k_{off} values of ZnAFs are strongly dependent on the Zn^{2+} chelating structure. The k_{off} values of higher affinity sensors, such as ZnAF-2 or ZnAF-2M, may be relatively small but are not too slow for reversible assay of Zn^{2+} concentration. It is also clear that low-affinity sensors are more suitable for monitoring Zn^{2+} in a reversible fashion because of their large k_{off} values.

Metal Ion Selectivity. Figure 4 illustrates the fluorescence intensity of ZnAFs in the presence of various metal ions. Like

(26) Miura, T.; Urano, Y.; Tanaka, K.; Nagano, T.; Ohkubo, K.; Fukuzumi, S. *J. Am. Chem. Soc.* **2003**, *125*, 8666–8671.